

A flexible Bayesian hierarchical modeling framework for spatially dependent peaks-over-threshold data

Rishikesh Yadav¹, Raphaël Huser¹ and Thomas Opitz²

December 20, 2021

Abstract In this work, we develop a constructive modeling framework for extreme threshold exceedances in repeated observations of spatial fields, based on general product mixtures of random fields possessing light or heavy-tailed margins and various spatial dependence characteristics, which are suitably designed to provide high flexibility in the tail and at sub-asymptotic levels. Our proposed model is akin to a recently proposed Gamma-Gamma model using a ratio of processes with Gamma marginal distributions, but it possesses a higher degree of flexibility in its joint tail structure, capturing strong dependence more easily. We focus on constructions with the following three product factors, whose different roles ensure their statistical identifiability: a heavy-tailed spatially-dependent field, a lighter-tailed spatially-constant field, and another lighter-tailed spatially-independent field. Thanks to the model’s hierarchical formulation, inference may be conveniently performed based on Markov chain Monte Carlo methods. We leverage the Metropolis adjusted Langevin algorithm (MALA) with random block proposals for latent variables, as well as the stochastic gradient Langevin dynamics (SGLD) algorithm for hyperparameters, in order to fit our proposed model very efficiently in relatively high spatio-temporal dimensions, while simultaneously censoring non-threshold exceedances and performing spatial prediction at multiple sites. The censoring mechanism is applied to the spatially independent component, such that only univariate cumulative distribution functions have to be evaluated. We explore the theoretical prop-

¹Computer, Electrical and Mathematical Sciences and Engineering (CEMSE) Division, King Abdullah University of Science and Technology (KAUST), Thuwal 23955-6900, Saudi Arabia. E-mails: rishikesh.yadav@kaust.edu.sa; raphael.huser@kaust.edu.sa

²INRAE, UR546 Biostatistics and Spatial Processes, 228, Route de l’Aérodrome, CS 40509, 84914 Avignon, France. E-mail: thomas.opitz@inra.fr

erties of the novel model, and illustrate the proposed methodology by simulation and application to daily precipitation data from North-Eastern Spain measured at about 100 stations over the period 2011–2020.

Keywords: Bayesian hierarchical modeling; extreme event; precipitation; stochastic gradient Langevin dynamics; sub-asymptotic modeling; threshold exceedance.

1 Introduction

Due to its importance in quantifying risk, the statistical modeling of extreme events is crucial in a wide range of environmental applications. Most environmental data are spatial or spatio-temporal in nature, and models at the interface between spatial statistics and Extreme-Value Theory (EVT) provide a mathematically rigorous way to study the marginal behavior of extreme events, while accounting for their potentially strong spatial or spatio-temporal dependence; see, e.g., the review papers by [Davison et al. \(2012\)](#), [Cooley et al. \(2012\)](#), [Davison and Huser \(2015\)](#), [Davison et al. \(2019\)](#). The block maximum (BM) and peaks-over-threshold (POT) approaches are the two principal techniques for modeling the extremes of a probability distribution. Although their pros and cons are still debated ([Bücher and Zhou, 2021](#)), the POT approach is usually preferred because of its more natural (and often better) use of available data, its direct modeling of the spatial extreme events that effectively took place, and its ability to model clusters of extreme events. The generalized Pareto (GP) distribution plays a key role in the POT approach, being the only possible limit for the marginal distribution of appropriately rescaled high threshold exceedances; see [Davison and Smith \(1990\)](#).

Various statistical approaches have been proposed for the modeling of spatial extremes, including Bayesian hierarchical models, copula models, max-stable random fields, and generalized Pareto processes; see the review papers by [Davison et al. \(2012\)](#) and [Huser and Wadsworth \(2020\)](#). Recently, Bayesian hierarchical models have gained in popularity for modeling spatial extremes

due to their flexibility to capture complex spatio-temporal trends, and their ease of inference in both BM and POT settings, when the data can be assumed to be conditionally independent given some spatially-structured latent variables. Conditional independence is a common assumption in Bayesian hierarchical models (Cressie, 1993; Cooley *et al.*, 2007; Banerjee *et al.*, 2014; Opitz *et al.*, 2018; Johannesson *et al.*, 2021) and drastically simplifies computations, but it also poses a risk of misrepresenting the data-level dependence structure. Based on this assumption, several Bayesian hierarchical models using latent variables have been proposed in the literature to model high threshold exceedances; see, e.g., Cooley *et al.* (2007), Opitz *et al.* (2018), Bacro *et al.* (2020), and the recent book chapter by Hazra *et al.* (2021). In particular, Cooley *et al.* (2007) used Gaussian processes to capture latent spatial dependence and trends in precipitation data, and used a relatively simple Markov chain Monte Carlo (MCMC) algorithm for the estimation of posterior distributions. Similarly, Turkman *et al.* (2010) fitted Bayesian hierarchical models to spatio-temporal wildfire data from Portugal by taking advantage of MCMC based inference, while Opitz *et al.* (2018) and Castro-Camilo *et al.* (2019) exploited the integrated nested Laplace approximation (INLA) to fit a model to spatio-temporal threshold exceedances. More recently, Hazra *et al.* (2021) proposed using Max-and-Smooth, an approximate Bayesian algorithm designed for extended latent Gaussian models and they applied it to a large-scale extreme precipitation dataset.

However, while these hierarchical models typically succeed in estimating marginal distributions accurately, the conditional independence assumption at the data level is very restrictive when the goal is to estimate return levels of spatial aggregates. Conditional independence models indeed yield unrealistic realizations for spatial phenomena such as rainfall or temperature, where threshold exceedances usually produce smooth surfaces (Ribatet *et al.*, 2012). Sang and Gelfand (2010) realized the limitation of the conditional independence model proposed by Sang and Gelfand (2009) and improved it by introducing a Gaussian copula at the data-level. Similarly, Clark and Dixon (2021) proposed spatial models based on self-exciting processes to capture strong spatial depen-

dence, allowing both data-level and latent-level dependencies.

As an alternative solution, in this work we extend the hierarchical modeling framework developed by [Yadav et al. \(2021\)](#) to capture relatively strong spatial dependence among threshold exceedances, by mixing several random fields multiplicatively in a way that ensures a heavy-tailed marginal behavior and generates a wide range of joint tail structures. To propose flexible heavy-tailed models, [Yadav et al. \(2021\)](#) relied on Breiman’s Lemma ([Breiman, 1965](#)), which characterizes the tail behavior of the product of two nonnegative independent random variables when one of them has power-law tail decay. Let X_1 and X_2 be nonnegative independent random variables such that $\mathbb{E}(X_1^{\alpha+\epsilon}) < \infty$, for some $\epsilon > 0$, and the distribution of X_2 is regularly varying at ∞ with index $-\alpha < 0$, i.e., $\Pr(X_2 > x) = \ell(x)x^{-\alpha}$, where $\ell(x) > 0$ and $\ell(tx)/\ell(t) \rightarrow 1$, as $t \rightarrow \infty$. Then, we have the expansion

$$\Pr(X_1 X_2 > x) \sim \mathbb{E}(X_1^\alpha) \Pr(X_2 > x), \quad x \rightarrow \infty. \quad (1)$$

Essentially, the result in (1) implies that the tail decay behavior of the product of two independent random variables, where one is regularly varying and other is lighter-tailed, is completely determined by the tail behavior of the regularly varying component, while the lighter-tailed component only contributes a constant scaling factor of tail probabilities. Breiman’s Lemma (1) motivates the construction of models with improved flexibility at a sub-asymptotic level, while allowing a heavy-tailed behavior. [Yadav et al. \(2021\)](#) used this result to generalize the GP distribution, which can be obtained from the product of two independent Exponential and Inverse Gamma-distributed random variables. Specifically, they proposed spatial models constructed as $Y(\mathbf{s}) = X_1(\mathbf{s})X_2(\mathbf{s})$, where $X_1(\mathbf{s})$ and $X_2(\mathbf{s})$ are independent processes that have Gamma and Inverse Gamma margins, respectively. While the light-tailed Gamma process $X_1(\mathbf{s})$ was assumed to be spatial white noise, the heavy-tailed Inverse Gamma process $X_2(\mathbf{s})$ was used to incorporate spatial dependence, thus inducing dependence among threshold exceedances. However, because of the spatial independence

of $X_1(\mathbf{s})$, the range of possible dependence structures that the product $Y(\mathbf{s}) = X_1(\mathbf{s})X_2(\mathbf{s})$ can attain is very limited, preventing the model from capturing strong tail dependence. This issue can also be seen by reformulating the process $Y(\mathbf{s})$ as a Bayesian hierarchical model, whereby $Y(\mathbf{s}) \mid X_2(\mathbf{s})$ is a conditionally independent Gamma process and $X_2(\mathbf{s})$ is a latent spatially-structured random field. The conditional independence assumption at the data-level here strongly restricts the form of dependence of $Y(\mathbf{s})$. In this paper, we generalize the hierarchical spatial model of [Yadav et al. \(2021\)](#) to provide new, more flexible hierarchical spatial models for threshold exceedances, that mitigate the effect of the conditional independence assumption at the data-level with the ultimate goal of capturing stronger spatial dependence among extreme events, while retaining the computational benefits and the intuitive interpretation of such Bayesian hierarchical models.

For the modeling of spatial precipitation (for which we usually find heavy tails), we consider instead the product of three suitably defined processes possessing different marginal and dependence characteristics, and with clearly distinct roles in the overall spatial model. More precisely, we assume that our model can be written as

$$Y(\mathbf{s}) = \alpha(\mathbf{s})X_1(\mathbf{s})X_2(\mathbf{s})X_3(\mathbf{s}), \quad (2)$$

where $X_1(\mathbf{s}) \geq 0$ is a unit mean noise process with independent and identically distributed (iid) variables that captures small scale variations and that allows fast Bayesian computations; $X_2(\mathbf{s}) \equiv X_2 \geq 0$ is a fully dependent spatial process with unit mean, which counterbalances the noise process $X_1(\mathbf{s})$ in case of strong dependence; $X_3(\mathbf{s}) \geq 0$ is a spatial process with unit mean and non-trivial spatial dependence structure, which captures the decay of spatial dependence with respect to spatial distance; $X_1(\mathbf{s})$, $X_2(\mathbf{s})$ and $X_3(\mathbf{s})$ are mutually independent; and $\alpha(\mathbf{s}) > 0$ is a spatially-varying scale parameter capturing non-stationarity in terms of covariates, where $\alpha(\mathbf{s}) = \mathbb{E}[Y(\mathbf{s})]$ owing to the unit mean condition on the random product terms; see [Section 2.1](#) for more details. Through their marginal distributions, these three underlying random processes are appropriately weighted

to determine the extent to which they contribute to the overall product mixture. We carefully design the roles of the three components to ensure their identifiability and to allow for meaningful interpretations. Our constructive modeling framework provides flexible models for the upper tail, and sub-asymptotic levels, such that we can use them for modeling complete datasets with heavy-tailed margins and moderate to strong upper tail dependence. In our models, the strength of tail dependence relies on the choice of the underlying copula in the latent process $X_3(\mathbf{s})$, and this gives flexibility to capture various asymptotic dependence regimes; see Section 2.3 for more details.

In this work, we focus on modeling heavy-tailed data, though the model could also be adapted to light tails with exponential decay by switching to an additive structure via a logarithmic transformation of (2), i.e., the data would be represented as $\log \alpha(\mathbf{s}) + \log X_1(\mathbf{s}) + \log X_2(\mathbf{s}) + \log X_3(\mathbf{s})$. Negative values can arise in this construction, but this can be avoided by considering the so-called softplus transformation $\log(1 + Y(\mathbf{s}))$ instead of $\log Y(\mathbf{s})$, with $Y(\mathbf{s})$ as in (2).

To fit our model to threshold exceedances $Y(\mathbf{s}) > u(\mathbf{s})$, where $u(\mathbf{s})$ is some high spatially-varying threshold, we take advantage of the hierarchical formulation of our model, and we exploit customized MCMC methods. Specifically, we use the simulation-based Metropolis adjusted Langevin algorithm (MALA) with random block proposals for latent parameters, as well as the stochastic gradient Langevin dynamics (SGLD) algorithm (Welling and Teh, 2011) for hyperparameters. The SGLD algorithm combines the popular stochastic gradient descent algorithm, known as an important optimization method in Machine Learning (Neal, 2012; Deng et al., 2018; Zhang et al., 2020), and the Langevin dynamics (Neal, 2011), to tackle problems in relatively high spatio-temporal dimensions. The SGLD algorithm indeed significantly reduces the computation burden to fit our model to threshold exceedances, and allows inference for massive datasets, by contrast to alternative, more classical inference methods for extreme-value POT models (Thibaud and Opitz, 2015; de Fondeville and Davison, 2018; Huser and Wadsworth, 2019). In our modeling framework, low values such that $Y(\mathbf{s}) \leq u(\mathbf{s})$ are completely censored in the MCMC algorithm. This censoring

mechanism can be performed very efficiently thanks to the independent noise component $X_1(\mathbf{s})$ in (2); see also [Zhang et al. \(2021\)](#) for a related censored inference approach.

The paper is organized as follows. In Section 2, we define our general product mixture model for spatial extremes with a specific example and study its joint tail behavior. In Section 3, we provide censored likelihood expressions for the product mixture model and a simulation study to check the performance of the MCMC sampler that are based on the MALA/SGLD algorithm, and in Section 4, we fit our model to daily mean precipitation intensities in North-Eastern Spain observed at 94 monitoring stations. Conclusions and some future research directions are detailed in Section 5.

2 Product mixture models for spatial threshold exceedances

2.1 General construction

Let $Y_t(\mathbf{s})$, $\mathbf{s} \in \mathcal{S} \in \mathbb{R}^2$, be the spatial process of interest observed at time $t \in \{1, \dots, n\}$ and at finite set of d locations $\mathbf{s}_1, \dots, \mathbf{s}_d \in \mathcal{S}$, and let the random vector $\mathbf{Y}_t = (Y_{t1}, \dots, Y_{td})^T = \{Y_t(\mathbf{s}_1), \dots, Y_t(\mathbf{s}_d)\}^T$ denote the t^{th} observed time replicate. We assume that the processes $Y_t(\mathbf{s})$, $t = 1, \dots, n$, are iid copies of the process $Y(\mathbf{s})$ in (2), such that $Y_t(\mathbf{s}) = \alpha(\mathbf{s})X_{1t}(\mathbf{s})X_{2t}(\mathbf{s})X_{3t}(\mathbf{s})$, for some non-negative independent processes $X_{1t}(\mathbf{s})$, $X_{2t}(\mathbf{s})$ and $X_{3t}(\mathbf{s})$. Similarly, we write $\mathbf{X}_{1t} = (X_{1t1}, \dots, X_{1td})^T = \{X_{1t}(\mathbf{s}_1), \dots, X_{1t}(\mathbf{s}_d)\}^T$, $\mathbf{X}_{2t} = (X_{2t1}, \dots, X_{2td})^T = \{X_{2t}(\mathbf{s}_1), \dots, X_{2t}(\mathbf{s}_d)\}^T$, $\mathbf{X}_{3t} = (X_{3t1}, \dots, X_{3td})^T = \{X_{3t}(\mathbf{s}_1), \dots, X_{3t}(\mathbf{s}_d)\}^T$, and $\boldsymbol{\alpha} = (\alpha_1, \dots, \alpha_d)^T = \{\alpha(\mathbf{s}_1), \dots, \alpha(\mathbf{s}_d)\}^T$. We now describe each of the terms in this product mixture. We assume that $X_{1t}(\mathbf{s})$ is a noise process such that the variables $X_{1t}(\mathbf{s}_j)$ are iid with distribution function F_1 and mean one, i.e., $\mathbb{E}(X_{1tj}) = 1$, for $j = 1, \dots, d, t = 1, \dots, n$. We further assume that $X_{2t}(\mathbf{s})$ is spatially constant, such that, almost surely, $X_{2t1} = \dots = X_{2td} \equiv X_{2t} \stackrel{iid}{\sim} F_2$, for some distribution F_2 , and that $\mathbb{E}(X_{2t}) = 1, t = 1, \dots, n$. Specifically, we assume that F_1 and F_2 have Weibull-like tails, i.e., $1 - F_1(x) \sim x^\eta \exp\{-(x/\lambda)^\kappa\}$, as $x \rightarrow \infty$, for some $\eta \in \mathbb{R}$, $\lambda > 0$ and $\kappa > 0$, and similarly for F_2 . Finally, we assume that $X_{3t}(\mathbf{s})$ is a non-trivial spatial process such that $\mathbf{X}_{3t} \stackrel{iid}{\sim} F_{\mathbf{X}_3}$, where the joint

distribution $F_{\mathbf{X}_3}$ has an underlying copula $C_{\mathbf{X}_3}$ (i.e., multivariate distribution with fixed uniform margins) and regularly varying marginal distribution, F_3 , with index $-1/\xi < 0$, for some $0 < \xi < 1$, and $\mathbb{E}(X_{3tj}) = 1$, $j = 1, \dots, d$, $t = 1, \dots, n$. Thus, we have that $1 - F_1(x) = o(1 - F_3(x))$ and $1 - F_2(x) = o(1 - F_3(x))$, as $x \rightarrow \infty$. We assume that the three random fields $X_{1t}(\mathbf{s})$, $X_{2t}(\mathbf{s})$, and $X_{3t}(\mathbf{s})$ are mutually independent (also across time t). As for the spatially-varying scale parameter $\alpha(\mathbf{s})$, we model it with covariates through a log-link function. Therefore, our general product mixture model is defined at the observed sites as

$$\mathbf{Y}_t = \boldsymbol{\alpha} \mathbf{X}_{1t} \mathbf{X}_{2t} \mathbf{X}_{3t}, \quad t = 1, \dots, n, \quad (3)$$

where $\boldsymbol{\alpha} = \exp(\gamma_0 \mathbf{1} + \gamma_1 \mathbf{Z}_1 + \dots + \gamma_p \mathbf{Z}_p)$ is the scale vector, $\mathbf{Z}_1, \dots, \mathbf{Z}_d$ are spatial covariates measured at the d locations, $\gamma_0, \dots, \gamma_p$ are the corresponding regression coefficients, n denotes the total number of independent time replicates, and operations are done componentwise. By construction, the mean of the observed vector \mathbf{Y}_t in (3) is $\mathbb{E}(\mathbf{Y}_t) = \boldsymbol{\alpha}$, and the marginal tail index is ξ (thanks to Breiman's Lemma (1)). The three random vectors in the product model (3) are designed to have distinct roles and capture different characteristics. Specifically, the random vector \mathbf{X}_{1t} is composed of iid variables, which allows us to capture small-scale variations and to perform fast Bayesian computations in case non-extreme observations are censored. The term \mathbf{X}_{2t} has a fully dependent spatial structure, which counterbalances the iid term \mathbf{X}_{1t} in case the data have an overall strong spatial dependence. Finally, \mathbf{X}_{3t} has a non-trivial spatial dependence structure, which is needed to capture the decay of spatial dependence with respect to distance. By suitably defining their marginal distributions, F_1 , F_2 , and F_3 , respectively, each of these random fields are appropriately weighted in our model with some “weight” parameters to be estimated from the data. A specific example is given in Section 2.2.

From (3), we can rewrite the spatial product mixture model hierarchically as follows:

$$Y_{tj} \mid \mathbf{X}_{2t}, \mathbf{X}_{3t}, \boldsymbol{\Theta}_{\mathbf{X}_1} \stackrel{\text{ind}}{\sim} F_1(\cdot / (\alpha_j X_{3tj} X_{2t}); \boldsymbol{\Theta}_{\mathbf{X}_1}), \quad j = 1, \dots, d, t = 1, \dots, n; \quad (4)$$

$$\begin{aligned}
X_{2t} \mid \Theta_{\mathbf{X}_2} &\stackrel{\text{ind}}{\sim} F_2(\cdot; \Theta_{\mathbf{X}_2}), \quad t = 1, \dots, n; \\
\mathbf{X}_{3t} \mid \Theta_{\mathbf{X}_3}^{\text{mar}^T}, \Theta_{\mathbf{X}_3}^{\text{dep}^T} &\stackrel{\text{ind}}{\sim} C_{\mathbf{X}_3} \left\{ F_3(\cdot; \Theta_{\mathbf{X}_3}^{\text{mar}}), \dots, F_3(\cdot; \Theta_{\mathbf{X}_3}^{\text{mar}}); \Theta_{\mathbf{X}_3}^{\text{dep}} \right\}; \\
\Theta &\sim \pi(\Theta),
\end{aligned}$$

where $\Theta = (\Theta_{\mathbf{X}_1}^T, \Theta_{\mathbf{X}_2}^T, \Theta_{\mathbf{X}_3}^{\text{mar}^T}, \Theta_{\mathbf{X}_3}^{\text{dep}^T})^T$ are the unknown model hyperparameters, $\Theta_{\mathbf{X}_1}$ and $\Theta_{\mathbf{X}_2}$ denote the hyperparameter vectors for the marginal distributions of the random vectors \mathbf{X}_{1t} and \mathbf{X}_{2t} , respectively, $\Theta_{\mathbf{X}_3} = (\Theta_{\mathbf{X}_3}^{\text{mar}^T}, \Theta_{\mathbf{X}_3}^{\text{dep}^T})^T$ contains parameters for the random vector \mathbf{X}_{3t} , with $\Theta_{\mathbf{X}_3}^{\text{mar}^T}$ controlling its marginal distribution and $\Theta_{\mathbf{X}_3}^{\text{dep}^T}$ controlling the dependence structure, $\pi(\Theta)$ denotes the prior distribution for the hyperparameter vector Θ , and α_j denotes the j^{th} parameter in the scale vector α .

The hierarchical construction of the proposed product model (4) suggests using Bayesian inference based on the full data vector $\mathbf{Y} = (\mathbf{Y}_1^T, \dots, \mathbf{Y}_n^T)^T$, by treating $\mathbf{X}_2 = (X_{21}, \dots, X_{2n})^T$ and $\mathbf{X}_3 = (\mathbf{X}_{31}^T, \dots, \mathbf{X}_{3n}^T)^T$ as latent variables. These two latent vectors, \mathbf{X}_2 and \mathbf{X}_3 , are of dimension n and nd , respectively. Therefore, there will be a total of $n + nd + |\Theta|$ latent variables and hyperparameters to make inference for, simultaneously. Let $\pi(\cdot)$ denote a generic (conditional) density, then the joint posterior density of Θ , \mathbf{X}_2 , and \mathbf{X}_3 , denoted by $\pi_{\text{post}}(\Theta, \mathbf{X}_2, \mathbf{X}_3 \mid \mathbf{Y})$, is proportional to $\pi(\mathbf{Y}, \Theta, \mathbf{X}_2, \mathbf{X}_3) = \pi(\mathbf{Y} \mid \mathbf{X}_2, \mathbf{X}_3, \Theta_{\mathbf{X}_1})\pi(\mathbf{X}_2 \mid \Theta_{\mathbf{X}_2})\pi(\mathbf{X}_3 \mid \Theta_{\mathbf{X}_3})\pi(\Theta)$, and the posterior density of Θ is thus obtained after integrating out the latent variables \mathbf{X}_2 and \mathbf{X}_3 , i.e.,

$$\pi(\Theta \mid \mathbf{Y}) = \iint \pi_{\text{post}}(\Theta, \mathbf{X}_2, \mathbf{X}_3 \mid \mathbf{Y}) d\mathbf{X}_2 d\mathbf{X}_3. \quad (5)$$

The dimension of the integral in (5) is very large. We solve this issue in Section 3.3 by using a customized MCMC algorithm by combining the Metropolis adjusted Langevin algorithm (MALA) with block proposals and the stochastic gradient Langevin dynamics (SGLD), in order to efficiently generate representative posterior samples of Θ , \mathbf{X}_2 , and \mathbf{X}_3 from the target posterior distribution.

2.2 An example of a flexible product mixture model

The general product mixture model formulation in (3) can be used to construct various specific spatial models with a flexible heavy-tailed behavior in the upper tail. Here, we provide one specific example of spatial product mixture model, which we also use in our simulation study in Section 2.3, and in the data application in Section 4. Let $\text{Exp}(1)$ denote the exponential distribution with rate parameter one. Then, a particular product mixture model can be obtained by specifying the terms in (3) as follows:

$$\begin{aligned} X_{1tj} &= E_{1tj}^{\beta_1} / \Gamma(1 + \beta_1), \quad E_{1tj} \stackrel{iid}{\sim} \text{Exp}(1), \quad j = 1 \dots, d, \quad t = 1, \dots, n, \quad \beta_1 > 0; \\ X_{2t} &= E_{2t}^{\beta_2} / \Gamma(1 + \beta_2), \quad E_{2t} \stackrel{iid}{\sim} \text{Exp}(1), \quad t = 1, \dots, n, \quad \beta_2 > 0, \end{aligned}$$

where $\Gamma(x) = \int_0^\infty s^{x-1} e^{-s} ds$ is the gamma function. The parameters β_1 and β_2 affect the marginal distributions of \mathbf{X}_{1t} and \mathbf{X}_{2t} , respectively, and can be interpreted as “weights” in the mixture (3), though they need not sum to one nor be less than one. As $\beta_1 \rightarrow 0$, the independent term \mathbf{X}_{1t} indeed becomes degenerate at one, and is thus negligible in the mixture (3). This holds similarly for the fully dependent term \mathbf{X}_{2t} , as $\beta_2 \rightarrow 0$. To ensure tails that are not heavier than exponential and/or to prevent potential numerical issues when computing the gradient of the log-posterior distribution (see Section 3 and the Supplementary Material), both β_1 and β_2 may be restricted to the range to $(0, 1]$, though this is not strictly necessary and in the application in Section 4.1 we allow slightly heavier-tailed distributions by restricting β_1 and β_2 to $(0, 2]$ instead. As for the random vector \mathbf{X}_{3t} , we define its marginal distribution F_3 to be the Inverse Gamma (IG) distribution with scale $\beta_3 - 1$, and shape β_3 , for some parameter $\beta_3 > 1$, such that $\mathbb{E}(X_{3tj}) = 1$, as desired. Moreover, as $\beta_3 \rightarrow \infty$, the term \mathbf{X}_{3t} becomes degenerate at one and does not have any effect on the mixture (3). Thus, this spatial model is more suitable for moderately heavy-tailed data with $\xi = 1/\beta_3 > 0$ (i.e.,

$\beta_3 < \infty$). In summary, the marginal distributions F_1 , F_2 and F_3 in (4) can be written as

$$F_1 = \text{Wb}\left\{ \cdot; \frac{1}{\beta_1}, \frac{1}{\Gamma(1 + \beta_1)} \right\}, F_2 = \text{Wb}\left\{ \cdot; \frac{1}{\beta_2}, \frac{1}{\Gamma(1 + \beta_2)} \right\}, F_3 = \text{IG}(\cdot; \beta_3, \beta_3 - 1), \quad (6)$$

where $\text{Wb}(\cdot; \kappa, \lambda)$ denotes the Weibull distribution with shape $\kappa > 0$ and scale $\lambda > 0$, and $\text{IG}(\cdot; a, b)$ denotes the Inverse Gamma distribution with shape $a > 0$ and scale $b > 0$. Furthermore, let the underlying copula $C_{\mathbf{X}_3}$ of \mathbf{X}_{3t} be the Gaussian copula with exponential correlation function $\rho(h) = \exp(-h/\rho)$, $h \geq 0$, and range $\rho > 0$. Then, \mathbf{X}_{3t} has joint distribution

$$\mathbf{X}_{3t} \mid \boldsymbol{\Theta}_{\mathbf{X}_3}^{\text{mar}^T}, \boldsymbol{\Theta}_{\mathbf{X}_3}^{\text{dep}^T} \sim \Phi_\rho \left(\Phi^{-1}[\text{IG}\{\cdot; \beta_3, \beta_3 - 1\}], \dots, \Phi^{-1}[\text{IG}\{\cdot; \beta_3, \beta_3 - 1\}] \right), \quad (7)$$

where Φ_ρ is the multivariate Gaussian distribution function with zero mean and correlation matrix $\boldsymbol{\Sigma}(\rho)$ with entries $\Sigma_{i_1, i_2} = \exp(-\|\mathbf{s}_{i_1} - \mathbf{s}_{i_2}\|/\rho)$, and Φ^{-1} is the quantile function of the standard Gaussian distribution. For this specific model, the hyperparameter vector is $\boldsymbol{\Theta} = (\boldsymbol{\Theta}_{\mathbf{X}_1}^T, \boldsymbol{\Theta}_{\mathbf{X}_2}^T, \boldsymbol{\Theta}_{\mathbf{X}_3}^{\text{mar}^T}, \boldsymbol{\Theta}_{\mathbf{X}_3}^{\text{dep}^T})^T$ with

$$\boldsymbol{\Theta}_{\mathbf{X}_1} = (\beta_1, \gamma_0, \gamma_1, \dots, \gamma_p)^T; \quad \boldsymbol{\Theta}_{\mathbf{X}_2} = \beta_2, \quad \boldsymbol{\Theta}_{\mathbf{X}_3}^{\text{mar}} = \beta_3, \quad \text{and} \quad \boldsymbol{\Theta}_{\mathbf{X}_3}^{\text{dep}} = \rho.$$

The marginal tail index for this model is $\xi = 1/\beta_3 > 0$, as the $\text{IG}(\cdot; a, b)$ distribution is regularly varying with index a . Therefore, as described, the marginal distribution of \mathbf{Y} is heavy-tailed, and the tail heaviness is controlled with the parameter β_3 .

It is of course also possible to consider alternative copula structures for \mathbf{X}_{3t} . A natural alternative, which produces asymptotic dependence in the data vector \mathbf{Y} , is the Student's t copula with dispersion matrix $\boldsymbol{\Sigma}(\rho)$ and degrees of freedom $\nu > 0$.

2.3 Joint tail behavior

We here derive the theoretical joint tail behavior of the spatial product mixture model (3) for the case where the latent vector \mathbf{X}_{3t} has a regularly varying marginal distribution with positive tail index $\xi > 0$ and \mathbf{X}_{1t} and \mathbf{X}_{2t} are lighter-tailed such that $\mathbb{E}\{(X_{1tj}X_{2tj})^{1/\xi+\epsilon}\} =$

$\mathbb{E}(X_{1tj}^{1/\xi+\varepsilon})\mathbb{E}(X_{2tj}^{1/\xi+\varepsilon}) < \infty$ for some $\varepsilon > 0$, which includes the example in Section 2.2. For convenience, we drop the subscript t in this subsection, so that the spatial product mixture model (3) may be generally written as $\mathbf{Y} = \boldsymbol{\alpha}\mathbf{X}_1\mathbf{X}_2\mathbf{X}_3$, with $\mathbf{X}_1, \mathbf{X}_2, \mathbf{X}_3$ defined as above. Furthermore, let the multivariate distribution $F_{\mathbf{X}_3}$ of \mathbf{X}_3 at a finite number of locations be (jointly) regularly varying at ∞ (Resnick, 1987) such that

$$\frac{1 - F_{\mathbf{X}_3}(z\mathbf{x}_3)}{1 - F_{\mathbf{X}_3}(z\mathbf{1})} \rightarrow V_{\mathbf{X}_3}(\mathbf{x}_3), \quad \mathbf{x}_3 > \mathbf{0}, \quad z \rightarrow \infty,$$

where $\mathbf{1} = (1, \dots, 1)^T \in \mathbb{R}^d$ and $V_{\mathbf{X}_3}(\mathbf{x}_3)$ is some positive limit function that is homogeneous of order $-1/\xi$, i.e., $V_{\mathbf{X}_3}(z\mathbf{x}_3) = z^{-1/\xi}V_{\mathbf{X}_3}(\mathbf{x}_3)$ for all $\mathbf{x}_3 > \mathbf{0}$ and $z > 0$. Then, Theorem 3 of Fougères and Mercadier (2012) implies the multivariate regular variation of $F_{\mathbf{Y}}$, which denotes the multivariate distribution of the data vector \mathbf{Y} , i.e.,

$$\frac{1 - F_{\mathbf{Y}}(z\mathbf{y})}{1 - F_{\mathbf{Y}}(z\mathbf{1})} \rightarrow V_{\mathbf{Y}}(\mathbf{y}) = \int_0^\infty \int_0^\infty \cdots \int_0^\infty V_{\mathbf{X}_3}\{\mathbf{y}/(\boldsymbol{\alpha}x_2\mathbf{x}_1)\} \left(\prod_{j=1}^d dF_1(x_{1j}) \right) dF_2(x_2), \quad z \rightarrow \infty, \quad (8)$$

where $V_{\mathbf{Y}}(\cdot)$ is some positive limit function that is also homogeneous of order $-1/\xi$. Equation (8) fully characterizes the extremal dependence of the product mixture \mathbf{Y} resulting from (3) in the heavy-tailed case. More, explicitly, the bivariate random vector $\mathbf{Y} = (Y_1, Y_2)^T$ is asymptotically independent if and only if $\mathbf{X}_3 = (X_{31}, X_{32})^T$ is asymptotically independent. Therefore, the asymptotic dependence class of the product mixture \mathbf{Y} depends on the choice of copula in the latent vector \mathbf{X}_3 . For example, \mathbf{Y} is asymptotically independent when we use a Gaussian copula in \mathbf{X}_3 and asymptotically dependent when we use a Student's t copula with $\nu > 0$ degrees of freedom instead.

Let $Y_1 \sim F_{Y_1}$ and $Y_2 \sim F_{Y_2}$, then a summary of the extremal dependence strength is the tail correlation coefficient $\chi = \lim_{u \rightarrow 1} \chi(u)$, where $\chi(u) = \Pr\{Y_1 > F_{Y_1}^{-1}(u) \mid Y_2 > F_{Y_2}^{-1}(u)\}$. We now study the strength of extremal dependence of the product mixture model defined in Section 2.2 in terms of the coefficients $\chi(u)$ and χ when using a latent Gaussian copula, or a latent Stu-

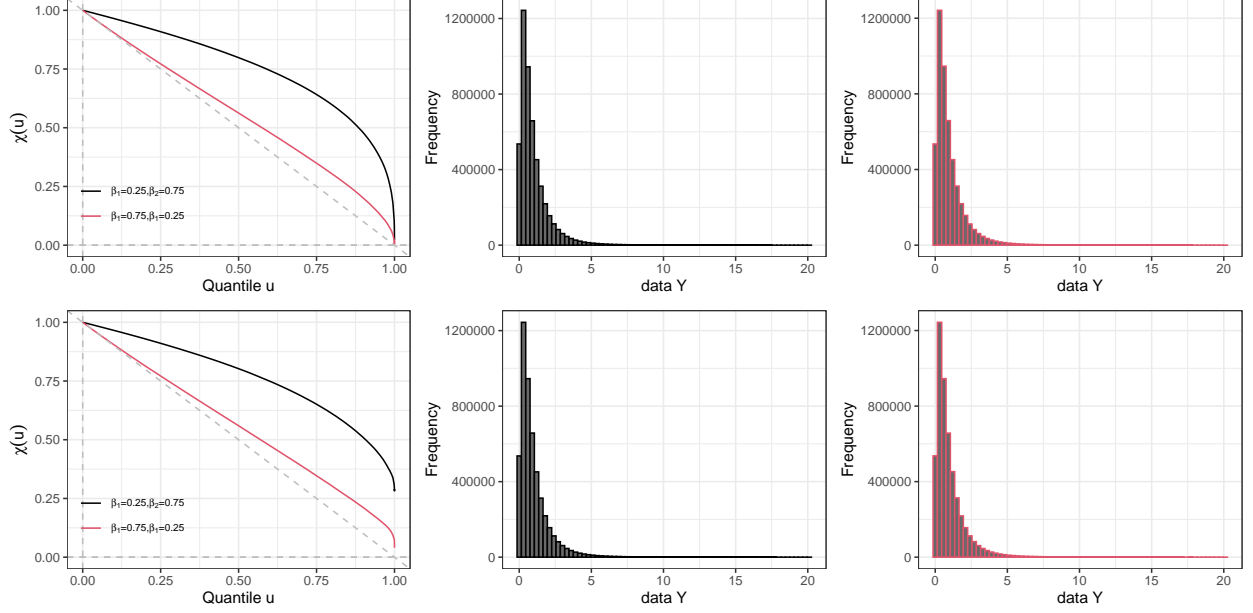


Figure 1: Plot of $\chi(u)$ (first column) for the product mixture model (3) with specific structure detailed in Section 2.2, based on a latent Gaussian copula (top) or Student’s t copula (bottom), with parameters chosen as $(\beta_1, \beta_2) = (0.25, 0.75)$ (black) or $(0.75, 0.25)$ (red), $\alpha_1 = \alpha_2 = 1$, $\beta_3 = 5$, $\rho = 1$, and for Student’s t case, $\nu = 1$, as well as the respective marginal histograms (second and third columns).

dent’s t copula with $\nu > 0$ degrees of freedom. Figure 1 shows the plot of $\chi(u)$ as a function of u and its limit χ (first column), and the marginal histogram (last two-columns) when using a latent Gaussian copula (first row) and latent Student’s t copula (second row), with an underlying exponential correlation function with range $\rho = 1$, at a spatial distance 0.5 (i.e., for a correlation of $\exp(-0.5) \approx 0.61$ in the latent vector \mathbf{X}_3). The other hyperparameters are set as follows: $\alpha_1 = \alpha_2 = 1$, $(\beta_1, \beta_2)^T = (0.25, 0.75)^T$ or $(0.75, 0.25)^T$, and for the Student’s t case, $\nu = 1$. These plots demonstrate that our product model can indeed capture various tail dependence decays, with stronger tail dependence when β_2 is higher. This is expected as β_2 is the “weight” associated with the fully dependent term \mathbf{X}_2 in the mixture model described in Section 2.2. Also, all the histograms appear to be quite similar to each other, which shows that the different parameter combinations give flexibility to capture different types of joint tail behavior, while the marginal tail behavior remains relatively unaffected when the scale parameters α_1, α_2 , and the shape parameter β_3 (i.e.,

the reciprocal of the tail index) are kept fixed. Moreover, as expected, the dependence strength of the data vector \mathbf{Y} depends on the choice of the copula in the latent vector \mathbf{X}_3 , i.e., the limiting tail correlation coefficient, χ , is strictly positive when we use a latent Student's t copula, whereas $\chi = 0$ when we use a latent Gaussian copula instead.

3 Simulation-based Bayesian inference

3.1 General strategy

The hierarchical construction (4) of our proposed spatial product mixture model (3) naturally suggests using simulation-based Bayesian inference where latent variables are simulated conditional to observations. We use Markov chain Monte Carlo (MCMC) methods to simultaneously generate samples of the hyperparameter vector Θ and the two latent parameter vectors, \mathbf{X}_2 and \mathbf{X}_3 . As we fit our model to threshold exceedances, we describe in Section 3.2 the censoring mechanism focusing on the specific model described in Section 2.2. In Section 3.3, we detail our MCMC sampler combining block Metropolis adjusted Langevin algorithm (MALA) updates for latent variables and the stochastic gradient Langevin dynamics (SGLD) for hyperparameters. We demonstrate the performance of our MCMC sampler based on a simulation study in Section 3.4.

3.2 Censored likelihood with latent variables, priors, and posterior density

We follow the notation of Section 2.1, with lowercase letters denoting realized values, i.e., y_{tj} is the realization of $Y_{tj} = Y_t(\mathbf{s}_j)$, x_{1tj} is the realization of $X_{1tj} = X_{1t}(\mathbf{s}_j)$, and so forth. Let $\mathbf{e}_t = (e_{t1}, \dots, e_{td})^T$ be the exceedance indicator vector, such that $e_{tj} = 1$, if $y_{tj} > u_{tj}$, and $e_{tj} = 0$, if $y_{tj} \leq u_{tj}$, where $\mathbf{u}_t = (u_{t1}, \dots, u_{td})^T$ is a fixed threshold vector. If $u_{tj} = 0$, no censoring is applied to the value y_{tj} , whereas if $u_{tj} = \infty$, the observation y_{tj} is treated as fully censored and as a variable to predict. Then, the augmented censored likelihood contribution for the parameter $(\Theta^T, x_{2t}, \mathbf{x}_{3t}^T)^T$, based on the data vector $(\mathbf{y}_t^T, \mathbf{e}_t^T)^T$, which stems from the general product mixture

model (3) with an underlying copula $C_{\mathbf{X}_3}$ (with density $c_{\mathbf{X}_3}$), is

$$\begin{aligned}
L(\boldsymbol{\Theta}, x_{2t}, \mathbf{x}_{3t}; \mathbf{y}_t, \mathbf{e}_t) &= \prod_{j=1}^d \left\{ \frac{1}{\alpha_j x_{2t} x_{3t}} f_1 \left(\frac{y_{tj}}{\alpha_j x_{2t} x_{3tj}}; \boldsymbol{\Theta}_{\mathbf{X}_1} \right) \right\}^{\mathbb{I}(e_{tj}=1)} \\
&\times \prod_{j=1}^d \left\{ F_1 \left(\frac{u_{tj}}{\alpha_j x_{2t} x_{3tj}}; \boldsymbol{\Theta}_{\mathbf{X}_1} \right) \right\}^{\mathbb{I}(e_{tj}=0)} \\
&\times f_2(x_{2t}; \boldsymbol{\Theta}_{\mathbf{X}_2}) \\
&\times c_{\mathbf{X}_3} \left\{ F_3(x_{3t1}; \boldsymbol{\Theta}_{\mathbf{X}_3}^{\text{mar}}), \dots, F_3(x_{3td}; \boldsymbol{\Theta}_{\mathbf{X}_3}^{\text{mar}}); \boldsymbol{\Theta}_{\mathbf{X}_3}^{\text{dep}} \right\} \prod_{j=1}^d f_3(x_{3tj}; \boldsymbol{\Theta}_{\mathbf{X}_3}^{\text{mar}}), \quad (9)
\end{aligned}$$

where f_1 , f_2 and f_3 are the density functions corresponding to the cumulative distribution function F_1 , F_2 and F_3 , respectively, and $\mathbb{I}(\cdot)$ is the indicator function. The expressions in (9) correspond to the likelihood contribution of non-censored observations (first line) and censored observations (second line), to the likelihood contribution of the latent variable x_{2t} (third line) and the latent variable vector \mathbf{x}_{3t} (fourth line). In particular, when $C_{\mathbf{X}_3}$ is the Gaussian copula, the density $c_{\mathbf{X}_3}$ has the form

$$\phi_\rho \left\{ \Phi^{-1}(v_1), \dots, \Phi^{-1}(v_d) \right\} \left[\prod_{j=1}^d \phi \left\{ \Phi^{-1}(v_j) \right\} \right]^{-1}, \quad \mathbf{v} = (v_1, \dots, v_d)^T \in [0, 1]^d,$$

where ϕ_ρ and ϕ are the multivariate and univariate Gaussian densities corresponding to Φ_ρ and Φ introduced in (7). Assuming independent time replicates, the overall augmented censored likelihood is then

$$L(\boldsymbol{\Theta}, \mathbf{x}_2, \mathbf{x}_3; \mathbf{y}, \mathbf{e}) = \prod_{t=1}^n L(\boldsymbol{\Theta}, x_{2t}, \mathbf{x}_{3t}; \mathbf{y}_t, \mathbf{e}_t), \quad (10)$$

where $\mathbf{y} = (\mathbf{y}_1^T, \dots, \mathbf{y}_n^T)^T$ is the complete data vector, $\mathbf{x}_2 = (x_{21}, \dots, x_{2n})^T$, $\mathbf{x}_3 = (\mathbf{x}_{31}^T, \dots, \mathbf{x}_{3n}^T)^T$, and $\mathbf{e} = (\mathbf{e}_1^T, \dots, \mathbf{e}_n^T)^T$ is the complete threshold indicator vector. In particular, the overall augmented likelihood for the specific model in Section 2.2 may be obtained by using the distribution functions F_1 , F_2 , F_3 , and their corresponding density functions as specified in (6). Using (10), the

joint posterior of model parameters $(\Theta^T, \mathbf{x}_2^T, \mathbf{x}_3^T)^T$ may be written as

$$\pi_{\text{post}}(\Theta, \mathbf{x}_2, \mathbf{x}_3 \mid \mathbf{y}, \mathbf{e}) \propto L(\Theta, \mathbf{x}_2, \mathbf{x}_3; \mathbf{y}, \mathbf{e})\pi(\Theta). \quad (11)$$

For convenience, we assume independent vague prior distributions for the model hyperparameters. In particular, for the specific model in Section 2.2, we have $\pi(\Theta) = \pi(\gamma_0) \times \pi(\gamma_1) \times \cdots \times \pi(\gamma_p) \times \pi(\beta_1) \times \pi(\beta_2) \times \pi(\beta_3) \times \pi(\rho)$. In the application in Section 4.1, for instance, we choose a standard Gaussian distribution with mean 0 and variance 100 for all the covariate coefficients $\gamma_0, \gamma_1, \dots, \gamma_p$ controlling the scale vector $\boldsymbol{\alpha} = \exp(\gamma_0 \mathbf{1} + \gamma_1 \mathbf{Z}_1 + \cdots + \gamma_p \mathbf{Z}_p)$, a uniform distribution on $[0, 2]$ for the “weight” parameters β_1 and β_2 to prevent overly large values, a gamma distribution with shape 1/3 and rate 1/100 for β_3 (reciprocal tail index), and a uniform distribution on $[0, 2\delta]$ for ρ (range parameter), where δ is the maximum spatial distance between the stations.

3.3 Stochastic gradient Langevin dynamics (SGLD) algorithm

When writing the model hierarchically, there are two latent parameter vectors, \mathbf{x}_2 and \mathbf{x}_3 , of dimensions n and nd , respectively. MCMC computations are therefore quite involved, and MCMC chains might mix poorly when n and d are both large. To avoid this issue when the latent parameter vector is of very high dimension, a suitable choice of proposal distributions is required. The Langevin dynamics (Roberts and Tweedie (1996), Roberts and Rosenthal (1998)) provides an efficient way to define proposal distributions, by exploiting information from the gradient of the log-posterior density, and it generally works quite efficiently in reasonably large dimensions. Let $\pi(\mathbf{z} \mid \mathbf{y}_n)$ be an arbitrary target posterior density of m components $\mathbf{z} = (z_1, \dots, z_m)^T$ conditioned on n replicated observations $\mathbf{y}_n = (y_1, \dots, y_n)^T$. Then, the proposal distribution based on the Langevin dynamics require to fix a step size parameter $\tau > 0$, and to sample proposals \mathbf{z}^p from

$$\mathbf{z}^p \mid \mathbf{z} \sim \mathcal{N}\left(\mathbf{z} + \frac{\tau}{2} P \nabla_{\mathbf{z}} \log \pi(\mathbf{z} \mid \mathbf{y}_n), \tau P\right), \quad (12)$$

where $\nabla_{\mathbf{z}}$ is the gradient operator with respect to the variable \mathbf{z} and τP is a covariance matrix; see [Atchadé \(2006\)](#). This algorithm is commonly called the Metropolis adjusted Langevin algorithm, MALA in short. If the dimension m is high, MALA proposals are feasible only if the gradient of the log-posterior density with respect to \mathbf{z} is available in closed form and can be computed efficiently. In our case, we have closed-form expressions of the log-posterior density with respect to both latent variable vectors \mathbf{x}_2 and \mathbf{x}_3 , and some hyperparameters, $\gamma_0, \gamma_1, \dots, \gamma_p, \beta_1$ and β_2 . For detailed calculations, see Sections 1.2 and 1.3 of the Supplementary materiel. One disadvantage of the classical MALA proposals, however, is that we need to compute the gradient of the log-posterior density at each MCMC iteration, which may be computationally prohibitive when the data dimension is large. To speed up computations, we instead rely on the SGLD algorithm. The latter may be significantly faster than the MALA, which uses the whole dataset at once (as, e.g., in [Yadav et al., 2021](#)). The stochastic gradient descent algorithm was popularized in Machine Learning for fitting complex Neural Network structures. Similarly, it is possible to exploit simulation-based MCMC inference based on the SGLD algorithm (a combination of stochastic gradient descent algorithm, and the Langevin dynamics), in order to speed up computations significantly. This method requires to select a batch size $b \in \{1, \dots, m\}$ and perform the updates based on a randomly selected sub-dataset of size b instead of the full dataset; for more details see [Nemeth and Fearnhead \(2020\)](#), and the pseudo-code in Algorithm 1. Intuitively, if $b \ll m$, then computations at each iteration will be much faster. More specifically, let $P = I_m$, then the proposal distribution (12) based on sub-dataset of size b may be written as

$$\mathbf{z}^p \mid \mathbf{z} \sim \mathcal{N} \left(\mathbf{z} + \frac{\tau n}{2b} \nabla_{\mathbf{z}}^* \log \pi(\mathbf{z} \mid \mathbf{y}_b), \tau \right), \quad (13)$$

where \mathbf{y}_b is the vector of length b sampled without replacement from the full data vector \mathbf{y}_n , and $\frac{n}{b} \nabla_{\mathbf{z}}^* \log \pi(\mathbf{z} \mid \mathbf{y}_b)$ is an unbiased estimator of $\nabla_{\mathbf{z}} \log \pi(\mathbf{z} \mid \mathbf{y}_n)$, based on \mathbf{y}_b only (i.e., it is computed from the summands in the gradient corresponding to \mathbf{y}_b , rescaled by n/b). It can be shown that the

Algorithm 1 Pseudo-code for the SGLD algorithm with Metropolis–Hastings correction

- 1: *Notation:* $P \setminus L$: set difference from P to L ; $|A|$ cardinality of the set A ; p : proposed states; c : current state
 - 2: *Input:* $\mathbf{y}_{[A_n, A_d]}$: data matrix of spatial dimension $|A_d|$ and temporal dimension $|A_n|$ where $A_d = \{1, \dots, d\}$ and $A_n = \{1, \dots, n\}$; Θ_k^0 , $\mathbf{x}_{2[A_n]}^0$, $\mathbf{x}_{3[A_n, A_d]}^0$: initial values for hyperparameter vector Θ_k , and latent parameter vectors \mathbf{x}_2 and \mathbf{x}_3 , respectively; b : batch size for the SGLD algorithm; N_{bn} : total burn-in samples (for simplicity, we here consider a single burn-in period); adapt: number of iterations after which we adapt the tuning parameters; $S_c = \{(c+0) \times \text{adapt}, (c+6) \times \text{adapt}, (c+12) \times \text{adapt}, \dots\}$, $c = 1, 2, 3, 4, 5, 6$; N_m : number of MCMC iterations after which we apply a Metropolis–Hastings correction; $N_h (= 4)$: number of blocks for hyperparameter vector Θ ; $N_{tot} = N \times N_m$: total number of MCMC iterations
 - 3: Start with $\Theta_k^{c'} = \Theta_k^0$, $\Theta_k^c = \Theta_k^0$, $\mathbf{x}_{2[A_n]}^c = \mathbf{x}_{2[A_n]}^0$, and $\mathbf{x}_{3[A_n, A_d]}^c = \mathbf{x}_{3[A_n, A_d]}^0$
 - 4: **for** $i = 1$ to N **do**
 - 5: **for** $j = 1$ to N_m **do**
 - 6: Sample random indices of length b from A_n without replacement, say the resulting set is $A_b = \{a_1, \dots, a_b\} \subset A_n$
 - 7: **for** $k = 1$ to N_h **do**
 - 8: *SGLD for Θ_k :* Propose (transformed) hyperparameter vector Θ_k^p using SGLD (13) with batch size b , i.e., based on observations $\mathbf{y}_{[A_b, A_d]}$, and set $\Theta_k^c = \Theta_k^p$ with probability one
 - 9: **end for**
 - 10: *Block MALA for \mathbf{x}_2 :* Propose (log-transformed) $\mathbf{x}_{2[A_b]}^p$ using SGLD (13) and calculate the acceptance ratio $r_{\mathbf{x}_2} = R_{\mathbf{x}_2}(\mathbf{x}_{2[A_b]}^p, \mathbf{x}_{2[A_b]}^c \mid \mathbf{y}_{[A_b, A_d]}, \mathbf{e}_{[A_b, A_d]}, \Theta^{c'}, \mathbf{x}_{3[A_b, A_d]}^c)$ using (15)
 - 11: Generate $U \sim U[0, 1]$, **if** $(U < r_{\mathbf{x}_2})$ $\{\mathbf{x}_{2[A_n]}^c = \mathbf{x}_{2[A_n \setminus A_b]}^c \cup \mathbf{x}_{2[A_b]}^p\}$ **else** $\{\mathbf{x}_{2[A_n]}^c = \mathbf{x}_{2[A_n]}^c\}$
 - 12: **if** $((i \times N_m < N_{bn}) \ \& \ (i \times N_m \in S_5))$ {use adaptive strategy to change the step size parameter} **else** {no change}
 - 13: *Block MALA for \mathbf{x}_3 :* Propose (log-transformed) $\mathbf{x}_{3[A_b, A_d]}^p$ using SGLD (13) and calculate the acceptance ratio $r_{\mathbf{x}_3} = R_{\mathbf{x}_3}(\mathbf{x}_{3[A_b, A_d]}^p, \mathbf{x}_{3[A_b, A_d]}^c \mid \mathbf{y}_{[A_b, A_d]}, \mathbf{e}_{[A_b, A_d]}, \mathbf{x}_{2[A_b]}^c, \Theta^{c'})$ using (16)
 - 14: Generate $U \sim U[0, 1]$, **if** $(U < r_{\mathbf{x}_3})$ $\{\mathbf{x}_{3[A_n, A_d]}^c = \mathbf{x}_{3[A_n \setminus A_b, A_d]}^c \cup \mathbf{x}_{3[A_b, A_d]}^p\}$ **else** $\{\mathbf{x}_{3[A_n, A_d]}^c = \mathbf{x}_{3[A_n, A_d]}^c\}$
 - 15: **if** $((i \times N_m < N_{bn}) \ \& \ (i \times N_m \in S_6))$ {use adaptive strategy to change the step size parameter} **else** {no change}
 - 16: **end for**
 - 17: **for** $k = 1$ to N_h **do**
 - 18: *Metropolis–Hastings correction for Θ_k :* Calculate the acceptance ratio $r_{\Theta_k} = R_{\Theta_k}(\Theta_k^c, \Theta_k^{c'} \mid \mathbf{y}_{[A_n, A_d]}, \mathbf{e}_{[A_n, A_d]}, \mathbf{x}_{2[A_n]}^c, \mathbf{x}_{3[A_n, A_d]}^c)$ using (14)
 - 19: Generate $U \sim U[0, 1]$, **if** $(U < r_{\Theta_k})$ $\{\Theta_k^{c'} = \Theta_k^c, \Theta_k^c = \Theta_k^{c'}\}$ **else** $\{\Theta_k^{c'} = \Theta_k^{c'}, \Theta_k^c = \Theta_k^{c'}\}$
 - 20: **if** $((i \times N_m < N_{bn}) \ \& \ (i \times N_m \in S_k))$ {use adaptive strategy to change the step size parameter} **else** {no change}
 - 21: **end for**
 - 22: **end for**
-

SGLD algorithm (13) has theoretical guarantees to converge to the exact stationary distribution

as the step size $\tau \equiv \tau_s \rightarrow 0$, such that $\sum \tau_s = \infty$ and $\sum \tau_s^2 < \infty$, where τ_s denote the step size at

s^{th} iteration; see [Welling and Teh \(2011\)](#) for more details. In practice, it is difficult to choose the optimal τ_s parameter as it relies on a bias variance trade-off, and is often chosen by cross-validation in the machine learning literature. As it is difficult to choose τ_s optimally in our complex models, we instead rely on the Metropolis–Hastings corrections applied after a fixed number of iterations. Here, we propose two different SGLD-based MCMC algorithms (i.e., Algorithm 1 and a simpler version thereof, Algorithm 2, described in the Supplementary Material) and we study their performance in our case by simulation in Section 3.4 and in the Supplementary Material. Note that, when the SGLD algorithm (13) is applied to the vector of latent variables in our model, the batch size b will be the same as the number of selected latent variables (involved in the selected batch), thus $n/b = 1$ in (13), and after Metropolis–Hastings corrections we may interpret it as a block MALA sampling scheme.

For conciseness, we here report only the details of Algorithm 1, which is based on the SGLD algorithm with Metropolis–Hastings corrections, as it turns out to be the best among the two proposed algorithms in terms of accuracy and computational cost. For details about the Algorithm 2, see Section 2 of the Supplementary Material.

Algorithm 1 is based on the SGLD algorithm and consists of three successive steps. Let the whole hyperparameter vector Θ be divided in four blocks as $\Theta = (\Theta_1^T, \Theta_2^T, \Theta_3^T, \Theta_4^T)^T$, where $\Theta_1 = (\gamma_0, \gamma_1, \dots, \gamma_p)^T$, $\Theta_2 = \beta_1$, $\Theta_3 = \beta_2$, and $\Theta_4 = (\beta_3, \rho)^T$. In the first step, we update the hyperparameters Θ_1 , Θ_2 , Θ_3 , and Θ_4 in four different blocks using the SGLD algorithm (13) with a random sub-dataset of size b . At every MCMC iteration, we propose a new state using the SGLD algorithm (13) and accept it with probability one, and then at the end of every fixed number (N_m) of iterations we either accept or reject the whole trajectory using the standard Metropolis–Hastings criterion; see the pseudo-code in Algorithm 1 for more details. In the second and third steps, we update a random subset of size b of the latent parameters \mathbf{x}_2 and \mathbf{x}_3 , respectively, through SGLD proposal (13), which is the same as using exact gradient

in (12), and after applying the Metropolis–Hastings correction it becomes a block MALA algorithm; see the pseudo-code in Algorithm 1 for more details. Denote $q_1(\Theta_k^p \mid \Theta_k)$, $q_2(\mathbf{x}_2^p \mid \mathbf{x}_2)$, and $q_3(\mathbf{x}_3^p \mid \mathbf{x}_3)$ the proposal distributions for the hyperparameter vector Θ_k , the latent parameter vector \mathbf{x}_2 , and the other latent parameter vector \mathbf{x}_3 , respectively, where the superscript p refers to proposal values. Let $\alpha_{\Theta_k}(\Theta_k^p, \Theta_k)$, $\alpha_{\mathbf{x}_2}(\mathbf{x}_2^p, \mathbf{x}_2)$, and $\alpha_{\mathbf{x}_3}(\mathbf{x}_3^p, \mathbf{x}_3)$ denote the acceptance probabilities for Θ_k , \mathbf{x}_2 , and \mathbf{x}_3 , respectively. Then, $\alpha_{\Theta_k}(\Theta_k^p, \Theta_k) = \min \{1, R_{\Theta_k}(\Theta_k^p, \Theta_k \mid \mathbf{y}, \mathbf{e}, \mathbf{x}_2, \mathbf{x}_3)\}$, $\alpha_{\mathbf{x}_2}(\mathbf{x}_2^p, \mathbf{x}_2) = \min \{1, R_{\mathbf{x}_2}(\mathbf{x}_2^p, \mathbf{x}_2 \mid \mathbf{y}, \mathbf{e}, \Theta, \mathbf{x}_3)\}$, $\alpha_{\mathbf{x}_3}(\mathbf{x}_3^p, \mathbf{x}_3) = \min \{1, R_{\mathbf{x}_3}(\mathbf{x}_3^p, \mathbf{x}_3 \mid \mathbf{y}, \mathbf{e}, \mathbf{x}_2, \Theta)\}$, where the corresponding acceptance ratios are

$$R_{\Theta_k}(\Theta_k^p, \Theta_k \mid \mathbf{y}, \mathbf{e}, \mathbf{x}_2, \mathbf{x}_3) = \frac{L\{(\Theta_k^p, \Theta_{-k}), \mathbf{x}_2, \mathbf{x}_3; \mathbf{y}, \mathbf{e}\} \pi(\Theta_k^p) q_1(\Theta_k \mid \Theta_k^p)}{L\{(\Theta_k, \Theta_{-k}), \mathbf{x}_2, \mathbf{x}_3; \mathbf{y}, \mathbf{e}\} \pi(\Theta_k) q_1(\Theta_k^p \mid \Theta_k)}, \quad k = 1, 2, 3, 4, \quad (14)$$

$$R_{\mathbf{x}_2}(\mathbf{x}_2^p, \mathbf{x}_2 \mid \mathbf{y}, \mathbf{e}, \Theta, \mathbf{x}_3) = \frac{L(\Theta, \mathbf{x}_2^p, \mathbf{x}_3; \mathbf{y}, \mathbf{e}) q_2(\mathbf{x}_2 \mid \mathbf{x}_2^p)}{L(\Theta, \mathbf{x}_2, \mathbf{x}_3; \mathbf{y}, \mathbf{e}) q_2(\mathbf{x}_2^p \mid \mathbf{x}_2)}, \quad (15)$$

$$R_{\mathbf{x}_3}(\mathbf{x}_3^p, \mathbf{x}_3 \mid \mathbf{y}, \mathbf{e}, \mathbf{x}_2, \Theta) = \frac{L(\Theta, \mathbf{x}_2, \mathbf{x}_3^p; \mathbf{y}, \mathbf{e}) q_3(\mathbf{x}_3 \mid \mathbf{x}_3^p)}{L(\Theta, \mathbf{x}_2, \mathbf{x}_3; \mathbf{y}, \mathbf{e}) q_3(\mathbf{x}_3^p \mid \mathbf{x}_3)}, \quad (16)$$

with $L(\Theta, \mathbf{x}_2, \mathbf{x}_3; \mathbf{y}, \mathbf{e})$ the censored likelihood in (9), and Θ_{-k} denotes the hyperparameter vector after removing the k^{th} block from the full hyperparameter vector Θ . The step size parameter τ in (13) determines the performance of the MCMC sampler and is directly responsible for jump sizes in the chains of $\{\Theta_k, k = 1, 2, 3, 4\}$, \mathbf{x}_2 and \mathbf{x}_3 at each MCMC iteration. Here, we have in fact six step size parameters to set, namely, $\{\tau_{\Theta_k}, k = 1, 2, 3, 4\}$, $\tau_{\mathbf{x}_2}$ and $\tau_{\mathbf{x}_3}$, corresponding to the SGLD updates for Θ_k s, \mathbf{x}_2 and \mathbf{x}_3 , respectively. We select them adaptively, throughout the MCMC algorithm, in order to achieve a desired acceptance probability. Let τ denote a generic step size parameter. We tune τ using the adaptive algorithm from Yadav et al. (2021): during an initial burn-in phase we modify the current value, τ_{cur} , of τ every 500 iterations as $\tau_{\text{cur}} \mapsto \tau_{\text{new}} := \exp \{(P_{\text{cur}} - P_{\text{tar}})/\theta\} \tau_{\text{cur}}$, where P_{tar} is the target acceptance probability, P_{cur} is the current acceptance probability (computed from the last 500 iterations), and $\theta > 0$ is a parameter fixed to modulate the rate of change of τ . Here, we set $P_{\text{tar}} = 0.23$ for random walk proposals and $P_{\text{tar}} = 0.57$ for SGLD based proposals. In a second burn-in phase, we update the tuning parameters using the same adaptive strategy only

if the acceptance probability drops out of the intervals $[0.15, 0.30]$ and $[0.50, 0.65]$ for random walk and SGLD based proposals, respectively.

Since all proposals are based on the Gaussian distribution, we transform the parameters so that their support becomes the whole real line through the following reparametrization:

$$\tilde{\gamma}_l = \gamma_l, l = 0, 1, \dots, p, \tilde{\beta}_1 = \log\left(\frac{\beta_1}{\delta_1 - \beta_1}\right), \tilde{\beta}_2 = \log\left(\frac{\beta_2}{\delta_2 - \beta_2}\right), \tilde{\beta}_3 = -\log(\beta_3 - 1), \tilde{\rho} = \log\left(\frac{\rho}{2\delta - \rho}\right).$$

where δ_1 and δ_2 are the upper limits for the β_1 and β_2 parameters, respectively, often set to some finite positive values (e.g., $\delta_1 = \delta_2 = 1$ or 2) to avoid numerical issues, and δ is the maximum distance between the stations (i.e., the “diameter” of the study region). The corresponding reverse transformation is

$$\gamma_l = \tilde{\gamma}_l, l = 0, 1, \dots, p, \tilde{\beta}_1 = \frac{\delta_1 \exp(\tilde{\beta}_1)}{1 + \exp(\tilde{\beta}_1)}, \tilde{\beta}_2 = \frac{\delta_2 \exp(\tilde{\beta}_2)}{1 + \exp(\tilde{\beta}_2)}, \beta_3 = 1 + \exp(-\tilde{\beta}_3), \rho = \frac{2\delta \exp(\tilde{\rho})}{1 + \exp(\tilde{\rho})}.$$

The Jacobian matrix of the transformation is $\log(J) = \log(\delta_1) + \tilde{\beta}_1 - 2\log\{1 + \exp(\tilde{\beta}_1)\} + \log(\delta_2) + \tilde{\beta}_2 - 2\log\{1 + \exp(\tilde{\beta}_2)\} - \tilde{\beta}_3 + \log(2) + \log(\delta) + \tilde{\rho} - 2\log\{1 + \exp(\tilde{\rho})\}$. Similarly, we log-transform the latent parameters as $\tilde{\mathbf{x}}_2 = \log(\mathbf{x}_2)$ and $\tilde{\mathbf{x}}_3 = \log(\mathbf{x}_3)$.

3.4 Simulation study

We now check the performance of our SGLD-based MCMC sampler (Algorithm 1) by simulation with respect to different batch sizes b . We also provide a simulation study for the comparison between the Algorithm 1 and Algorithm 2; for conciseness, the results are reported in the Supplementary material. We simulate data from the spatial product mixture model specified in Section 2.2 for $d = 100$ spatial locations and $n = 200$ time replicates (total $100 \times 200 + 200 = 20,200$ latent variables). The spatial locations are generated uniformly in the unit square $[0, 1]^2$ and the latent term \mathbf{X}_{3t} has an underlying Gaussian copula with a stationary isotropic exponential correlation function $\sigma(h) = \exp(-\|h\|/\rho)$, where $\rho > 0$ is the range parameter, set here to $\rho = 0.5$. For the purpose of spatial prediction, we completely mask the data at 20 sites, such that their simulated values

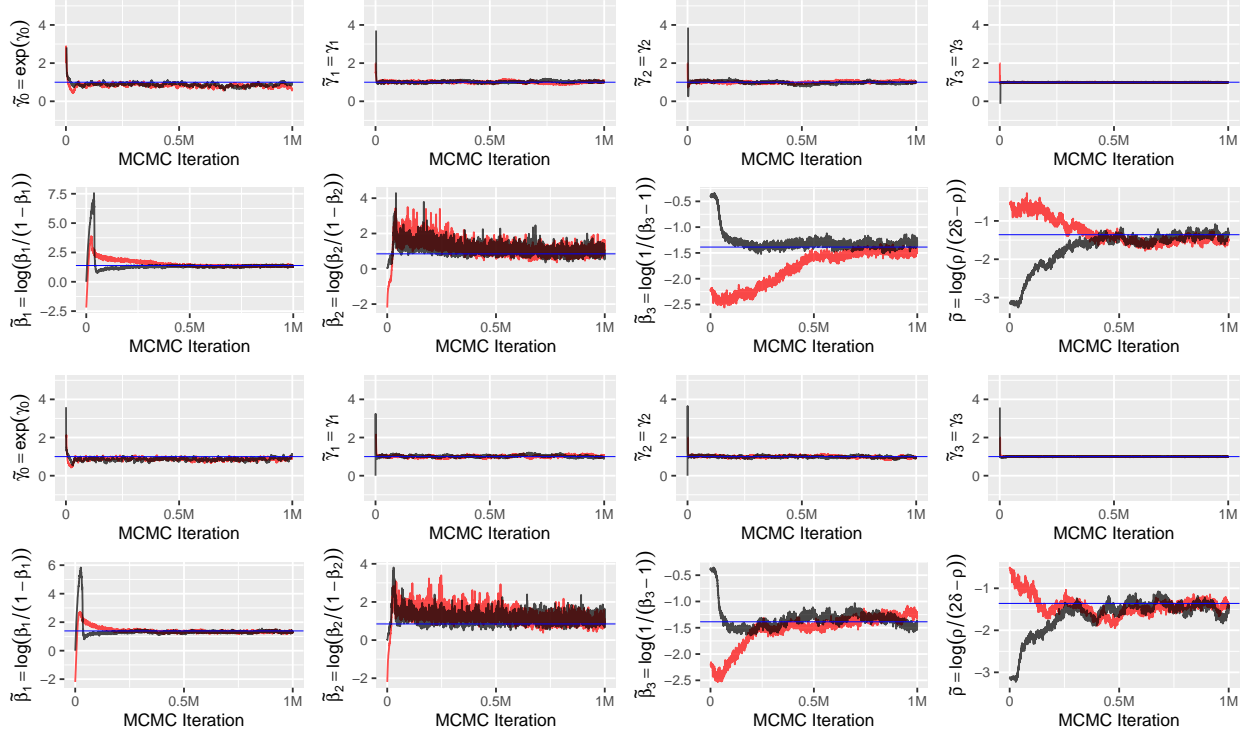


Figure 2: Trace plots for all hyperparameters in our simulation study. The first two rows correspond to the Algorithm 1 with batch size $b = 5$, and the last two rows are with batch size $b = 20$. The two Markov chains (red and black), correspond to two different initial values. The total number of MCMC sample iterations is 1 million (1M). The blue horizontal lines show the true values.

are treated as fully missing. The censoring threshold u_{tj} is here fixed to the site-wise 75% quantile based on the observations $(y_{1j}, \dots, y_{nj})^T$, and we set $u_{tj} = \infty$, whenever data y_{tj} is missing. The parameters are chosen as $\beta_1 = 0.8$, $\beta_2 = 0.7$, $\beta_3 = 5$ (i.e., $\xi = 0.2$), and the scale parameter is modeled spatially as $\alpha = \exp(\gamma_0 \mathbf{1} + \gamma_1 \mathbf{Z}_1 + \gamma_2 \mathbf{Z}_2 + \gamma_3 \mathbf{Z}_3)$, where $\exp(\gamma_0) = \gamma_1 = \gamma_2 = \gamma_3 = 1$, \mathbf{Z}_1 denotes the x -coordinate of each site, \mathbf{Z}_2 denotes the y -coordinate of each site, and \mathbf{Z}_3 is a covariate that is randomly generated from the standard normal distribution.

To make inference, we use the MCMC sampler detailed in Algorithm 1, where we set $N_m = 25$, $\delta_1 = \delta_2 = 1$, so that the parameters β_1 and β_2 lie within the interval $[0, 1]$, and δ is set to the maximum spatial distance between the observed locations. We run two MCMC chains in parallel with two different initial values to check the convergence of Markov chains, and we compute the posterior summaries by averaging values from the two Markov chains.

Table 1: Absolute bias, standard error, 95% credible interval (CI) length, effective sample size per minute (ESS/min.) for the SGLD-based MCMC algorithm (Algorithm 1) for different batch sizes $b = 5, 10, 20$ in our simulation study. All posterior summary statistics are calculated after removing the first $3N_{tot}/4$ burn-in samples, where $N_{tot} = 1$ million is the total number of MCMC iterations.

	batch size b	$\exp(\gamma_0)$	γ_1	γ_2	γ_3	β_1	β_2	β_3	ρ
Absolute bias	5	0.18	0.01	0	0.01	0.01	0.02	0.08	0.03
	10	0.09	0.02	0.04	0.01	0.01	0.07	0.13	0.04
	20	0.13	0.03	0.03	0.01	0.01	0.05	0.24	0.03
Standard error	5	0.06	0.03	0.03	0.01	0.01	0.03	0.16	0.02
	10	0.05	0.03	0.04	0.01	0.01	0.03	0.22	0.03
	20	0.05	0.03	0.04	0.01	0.01	0.03	0.16	0.03
95% CI length	5	0.23	0.12	0.1	0.04	0.02	0.13	0.61	0.08
	10	0.18	0.12	0.13	0.03	0.02	0.12	0.83	0.12
	20	0.2	0.12	0.14	0.03	0.03	0.12	0.65	0.12
ESS/min.	5	2.96	1.79	7.2	177.29	23.97	54.78	13.88	4.75
	10	9.66	1.69	2.25	150.67	16.43	57.35	2.41	2.23
	20	13.97	4.04	1.8	114.87	5.8	41.4	4.38	2.8

Figure 2 shows the trace plots for all hyperparameters for two different batch sizes b . The first two rows show the Markov chains for Algorithm 1 with batch size $b = 5$, and the last two rows correspond to batch size $b = 20$. For both batch sizes, the MCMC chains show good and comparable mixing performance and relatively fast convergence, especially for the regression parameters $\gamma_0, \gamma_1, \dots, \gamma_p$, as well as for the “weights” β_1 and β_2 . The parameters β_3 and ρ are slower to converge but they appear to suitably converge after about 0.5 million iterations. The true values for all hyperparameters are close to the posterior means with a relatively narrow 95% credible interval, suggesting that the MCMC algorithm performs well overall. The run-time is almost 9.5 hours to run 1 million iterations when the batch is size $b = 5$, and it takes about 14 hours to run 1 million iterations when the batch size is set to $b = 20$. Significant speed-up can thus be obtained without compromising much on the convergence of Markov chains. Table 1 compares the performance of the SGLD-based MCMC algorithm (Algorithm 1) with respect to different batch sizes, $b = 5, 10$ and 20 . The results are similar for different batch sizes, so in our application we choose the batch size $b = 5$ as it yields significant speed-up and the highest effective sample size per minute (ESS/min) for the hyperparameters that are the most tricky to estimate (i.e., β_1 , β_3 and ρ).

In Figure 3, we examine the predictive performance of our algorithm at the 20 unobserved sites

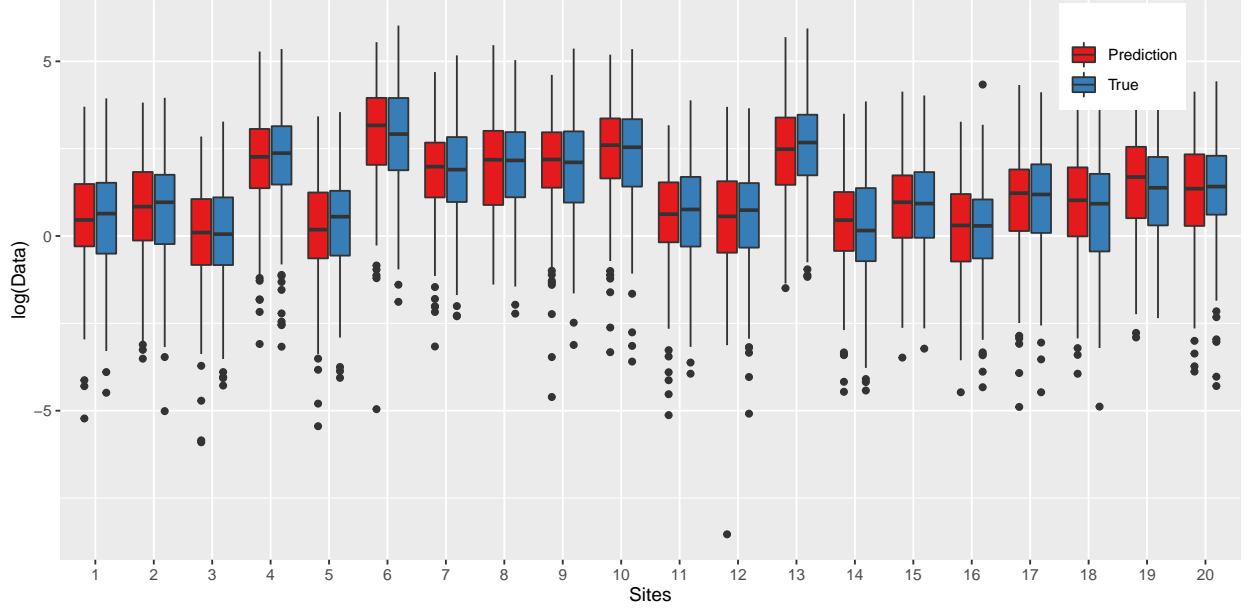


Figure 3: Boxplots of samples from the predictive distribution (red) at the 20 unobserved sites, along with boxplots of true (masked) observations at the same sites (blue), both in log scale. Here, the batch size of Algorithm 1 is set to $b = 5$.

(with masked observations) by comparing boxplots of the true (masked) observations to samples from the corresponding posterior predictive distribution. Samples from the posterior predictive distribution are obtained using the product mixture construction (3), where the model hyperparameters are estimated using the sample posterior median. The posterior predictive boxplots are similar to the boxplots of the true data, and capture the variability at each site quite well. This suggests that our algorithm succeeds in performing spatial prediction. Thanks to our model construction, it is possible to use our censored inference approach to simultaneously fit the model to high threshold exceedances and perform spatial prediction at unobserved locations efficiently.

4 Application to extreme precipitation data in Spain

4.1 Data description

To illustrate our methodology, we now study precipitation intensities from Spain, publicly available from the [European Climate Assessment and Dataset](#) project. The dataset reports daily precipitation amounts observed at more than 200 spatial locations from 1941 to 2018. We apply our spatial

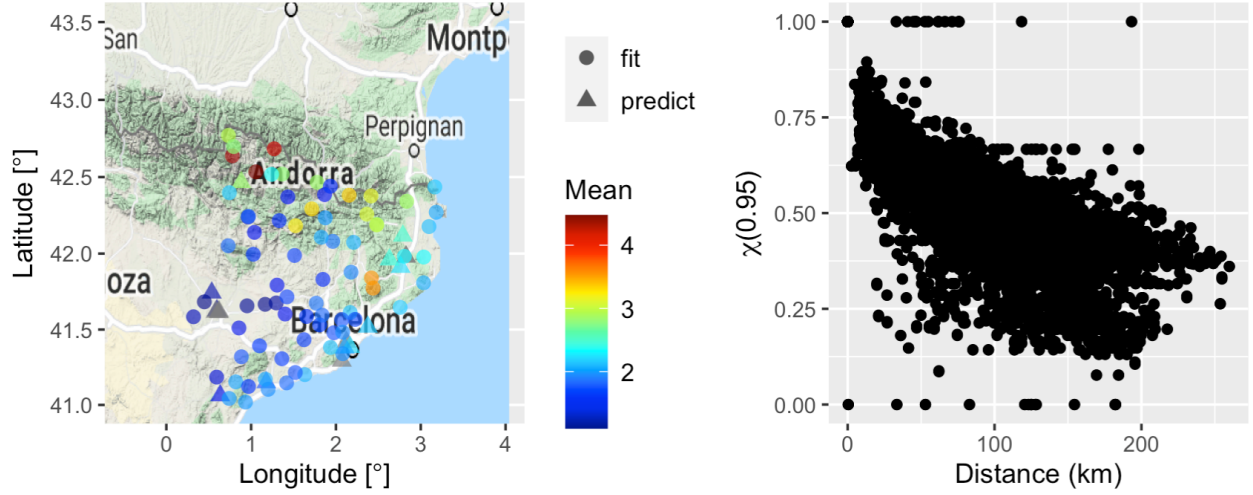


Figure 4: Left: Color-coded mean precipitation amount [mm] at the study sites. Dots represent sites used for fitting and triangles represent sites where spatial prediction is performed. Right: $\chi(u)$ plot at a fixed threshold $u = 0.95$.

product mixture model to a subset corresponding to a study region in North-Eastern Spain with $d = 94$ observation sites, and we consider the study period from 2011 to 2020. To avoid modeling complex temporal nonstationarities, we keep observations from September to December (i.e., the most rainy season), resulting in $n = 1220$ temporal replicates (total $94 \times 1220 + 1220 = 115,900$ latent variables). The distance between the two furthest sites is 260km, and the two closest sites are 0.17km apart. The site-wise proportion of missing observations varies from 0.01% to 100%. Also, the proportion of zeros at each site ranges from 41% to 85% with an average of 70%. The left panel in Figure 4 shows the site-wise mean precipitation plot, and the right panel shows the pairwise extremal correlation plot (i.e., $\chi(u)$ coefficient) at a fixed threshold $u = 95\%$. These plots show that there is considerably strong spatial heterogeneity and strong tail dependence in the data. The northern region receives higher precipitation than the southern region, and the sites at higher altitude receive higher precipitation, as well. This motivates including geographical information such as latitude, longitude and altitude, as covariates in the model.

4.2 Modeling precipitation intensities using the spatial product mixture models

We fit our specific spatial product model detailed in Section 2.2 to the Spanish precipitation data. Precisely, we consider several models where the scale vector α comprises linear or quadratic spatial covariates in terms of latitude (\mathbf{Z}_1), longitude (\mathbf{Z}_2), and altitude (\mathbf{Z}_3), where covariates are standardized to have mean zero and unit variance. We specifically consider the following models:

$$\text{M1: } \alpha = \exp(\gamma_0 \mathbf{1}_d)$$

$$\text{M2: } \alpha = \exp(\gamma_0 \mathbf{1}_d + \gamma_{\text{lat}} \mathbf{Z}_1)$$

$$\text{M3: } \alpha = \exp(\gamma_0 \mathbf{1}_d + \gamma_{\text{lat}} \mathbf{Z}_1 + \gamma_{\text{long}} \mathbf{Z}_2)$$

$$\text{M4: } \alpha = \exp(\gamma_0 \mathbf{1}_d + \gamma_{\text{lat}} \mathbf{Z}_1 + \gamma_{\text{long}} \mathbf{Z}_2 + \gamma_{\text{alt}} \mathbf{Z}_3)$$

$$\text{M5: } \alpha = \exp(\gamma_0 \mathbf{1}_d + \gamma_{\text{lat}} \mathbf{Z}_1 + \gamma_{\text{long}} \mathbf{Z}_2 + \gamma_{\text{alt}} \mathbf{Z}_3 + \gamma_{\text{lat}^2} \mathbf{Z}_1^2)$$

$$\text{M6: } \alpha = \exp(\gamma_0 \mathbf{1}_d + \gamma_{\text{lat}} \mathbf{Z}_1 + \gamma_{\text{long}} \mathbf{Z}_2 + \gamma_{\text{alt}} \mathbf{Z}_3 + \gamma_{\text{lat}^2} \mathbf{Z}_1^2 + \gamma_{\text{long}^2} \mathbf{Z}_2^2)$$

$$\text{M7: } \alpha = \exp(\gamma_0 \mathbf{1}_d + \gamma_{\text{lat}} \mathbf{Z}_1 + \gamma_{\text{long}} \mathbf{Z}_2 + \gamma_{\text{alt}} \mathbf{Z}_3 + \gamma_{\text{lat}^2} \mathbf{Z}_1^2 + \gamma_{\text{long}^2} \mathbf{Z}_2^2 + \gamma_{\text{alt}^2} \mathbf{Z}_3^2)$$

$$\text{M8: } \alpha = \exp(\gamma_0 \mathbf{1}_d + \gamma_{\text{lat}} \mathbf{Z}_1 + \gamma_{\text{long}} \mathbf{Z}_2 + \gamma_{\text{alt}} \mathbf{Z}_3 + \gamma_{\text{lat}^2} \mathbf{Z}_1^2 + \gamma_{\text{long}^2} \mathbf{Z}_2^2 + \gamma_{\text{alt}^2} \mathbf{Z}_3^2 + \gamma_{\text{lat.long}} \mathbf{Z}_1 \mathbf{Z}_2)$$

$$\text{M9: } \alpha = \exp(\gamma_0 \mathbf{1}_d + \gamma_{\text{lat}} \mathbf{Z}_1 + \gamma_{\text{long}} \mathbf{Z}_2 + \gamma_{\text{alt}} \mathbf{Z}_3 + \gamma_{\text{lat}^2} \mathbf{Z}_1^2 + \gamma_{\text{long}^2} \mathbf{Z}_2^2 + \gamma_{\text{alt}^2} \mathbf{Z}_3^2 + \gamma_{\text{lat.long}} \mathbf{Z}_1 \mathbf{Z}_2 + \gamma_{\text{long.alt}} \mathbf{Z}_2 \mathbf{Z}_3)$$

$$\text{M10: } \alpha = \exp(\gamma_0 \mathbf{1}_d + \gamma_{\text{lat}} \mathbf{Z}_1 + \gamma_{\text{long}} \mathbf{Z}_2 + \gamma_{\text{alt}} \mathbf{Z}_3 + \gamma_{\text{lat}^2} \mathbf{Z}_1^2 + \gamma_{\text{long}^2} \mathbf{Z}_2^2 + \gamma_{\text{alt}^2} \mathbf{Z}_3^2 + \gamma_{\text{lat.long}} \mathbf{Z}_1 \mathbf{Z}_2 + \gamma_{\text{long.alt}} \mathbf{Z}_2 \mathbf{Z}_3 + \gamma_{\text{lat.alt}} \mathbf{Z}_1 \mathbf{Z}_3)$$

The censoring threshold for each of the models M1–M10 is set to the 75% site-wise quantile of the strictly positive precipitation intensities. We choose 76 stations for fitting and leave 18 stations for prediction and model validation, where the true data are masked. For missing observations, we set the censoring threshold to $u_{tj} = \infty$. For inference, we use the SGLD-based scheme (Algorithm 1) presented in Section 3 with one million (1M) iterations, $N_m = 25$, and with a batch size of $b = 5$ for all the models. Also, we set $\delta_1 = \delta_2 = 2$, to avoid numerical issue and given that the data shows strong dependence, so that β_1 and β_2 parameters lies within the intervals $[0, 2]$.

Table 2 compares the model performances based on the mean squared prediction error (MPE), the continuous ranked probability score (CRPS; Gneiting and Raftery, 2007), and the tail-weighted CRPS (twCRPS; Lerch et al., 2017), averaged over the 18 prediction stations. Although model M3 is the best according to the CRPS and twCRPS criteria, it has surprisingly a huge MPE value.

Table 2: Mean squared prediction error (MPE) scores, continuous ranked probability score (CRPS), and tail-weighted CRPS scores, averaged over the 18 prediction stations, where the weight function in the twCRPS is chosen as the Gaussian distribution function with variance 100 and mean corresponding to the marginal threshold values. Lower values of (MPE), CRPS and twCRPS indicate better models, and the best performance for each criterion is highlighted in bold.

	M1	M2	M3	M4	M5	M6	M7	M8	M9	M10
MPE	3019.28	3046.96	3053.77	2501.67	2926.22	2900.99	2869.43	2733.31	2730.02	2730.63
CRPS	49.85	43.88	43.75	45.06	43.94	44.05	44.06	47.47	47.38	48.27
twCRPS	40.16	34.36	34.25	35.35	34.36	34.45	34.45	37.62	37.55	38.36

Table 3: Posterior summary statistics for our best model (M4), calculated based on $N_{tot}/4$ samples after deleting the first $3N_{tot}/4$ burn-in samples, where $N_{tot} = 1$ million is the total number of MCMC samples.

	$\exp(\gamma_0)$	γ_{lat}	γ_{long}	γ_{alt}	β_1	β_2	$\xi = 1/\beta_3$	ρ [km]
Post. mean	3.247	0.089	0.116	0.246	1.258	1.995	0.095	519.406
Standard dev.	0.062	0.023	0.027	0.019	0.011	0.005	0.002	0.046
Lower 95% CI	3.137	0.04	0.064	0.208	1.237	1.981	0.092	519.313
Upper 95% CI	3.31	0.13	0.163	0.279	1.288	2	0.089	519.337
ESS/min	0.253	73.05	155.365	57.434	13.293	155.365	0.396	1.131

Moreover, quantile-quantile (QQ) plots for model M3 (not shown) reveal that the marginal fit is poor at several stations. Therefore, we prefer to select model M4 as our best model, which is slightly more complex but has the lowest MPE and comparable CRPS and twCRPS values, and can adequately capture the complex spatially-varying dynamics of precipitation extremes. The total run-time for model M4 is approximately 28 hours to generate one million samples.

Table 3 shows posterior summary statistics for the best model M4. The estimates of covariate coefficients such as longitude ($\hat{\gamma}_{long} = 0.12$), latitude ($\hat{\gamma}_{lat} = 0.09$), and altitude ($\hat{\gamma}_{alt} = 0.25$), are highly significant, which shows that these geographical covariates are needed in the model. The estimate of β_2 is close to 2, which confirms that there is strong spatial dependence in the data and that the spatially constant term \mathbf{X}_{2t} in (3) is crucially needed. The estimate of β_1 is about 1.26, indicating that there is also non-negligible small-scale variability. The estimated tail index is $\hat{\xi} = 0.10$, indicating moderately heavy tails, which is in line with most precipitation data. The QQ-plots in Figure 5 show that the marginal predictive performance of our model is satisfactory. Figure 5 shows QQ-plots at all prediction stations where the data have been masked, and for some

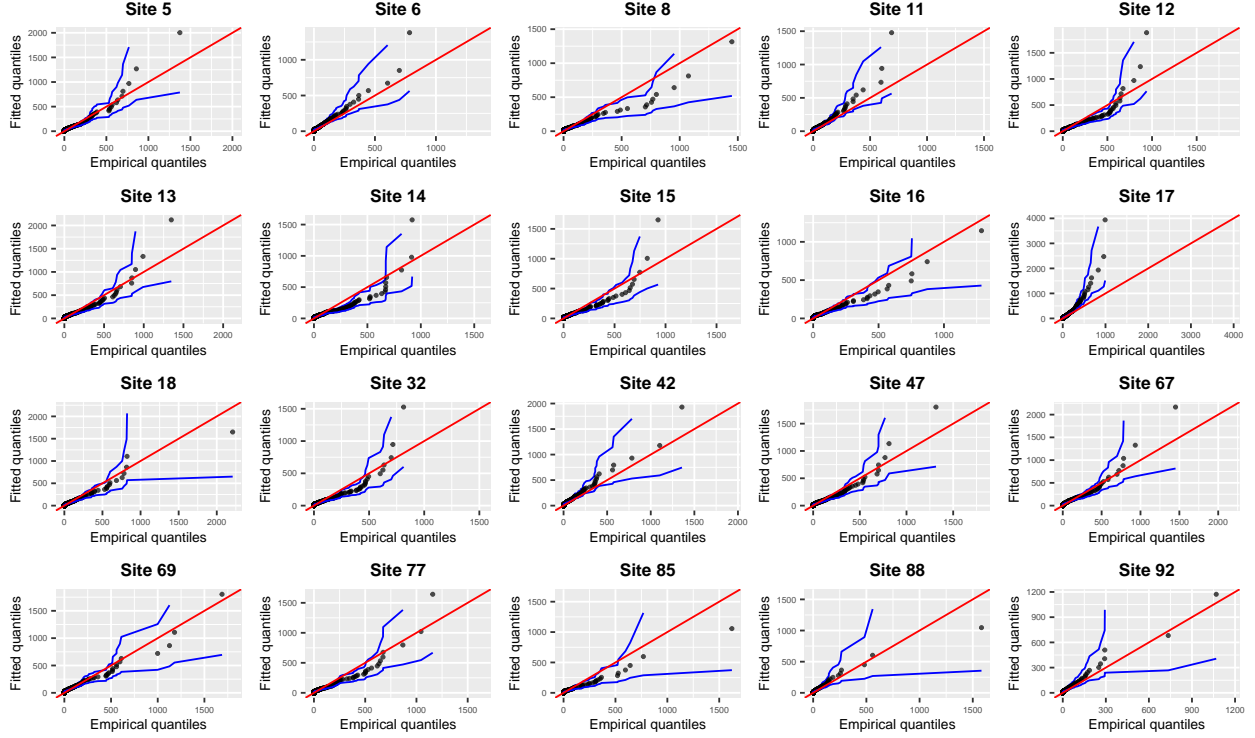


Figure 5: QQ-plots at all prediction stations where the data have been masked (up to site #18), and some selected fitted sites based on model M4. The fitted quantiles are simulated from the specific product model in Section 2.2, where the model hyperparameters are estimated using the corresponding posterior mean, calculated based on $N_{tot}/4$ samples after removing the first $3N_{tot}/4$ burn-in samples, where $N_{tot} = 1\text{M}$ is the total number of MCMC samples.

selected fitted stations. The estimated quantiles in this plot are obtained by simulation from the fitted product mixture model of Section 2.2, where the model hyperparameters are estimated using the posterior means of the corresponding posterior samples.

5 Conclusion

In this paper, we have provided a constructive modeling framework for extreme spatial threshold exceedances based on product mixtures of three distinct and mutually independent random fields, where each of the fields is characterized by a distinct combination of heavy- or lighter-tailed margins and spatial dependence characteristics. These models provide high flexibility in the tail and at sub-asymptotic levels and may be used to capture strong tail dependence in high threshold exceedances. The dependence strength of our proposed model depends on the choice of the underlying copula

structure at the latent level, and therefore we can get a variety of flexible dependence structures depending on the latent copula specification.

We here design an SGLD-based MCMC algorithm to fit our model efficiently in high spatio-temporal dimensions, where the dimension of the latent parameter vector is comparable to the data dimension. By using the SGLD algorithm, we bypass the expensive calculation of full censored-likelihood, and full gradients, and hence inference is significantly faster with high data dimensions. Thanks to the SGLD algorithm, we can indeed drastically reduce the computational cost of each MCMC iteration, allowing us to fit complex Bayesian hierarchical models with strong data-level tail dependence, to threshold exceedances in high dimensions.

In our data application, we have shown how to model precipitation extremes, and have illustrated our methodology on data from North-Eastern Spain. Although our methodology was illustrated with the specific spatial mixture model of Section 2.2, our constructive modeling framework is very general and can lead to several alternative heavy-tailed models. Future research directions include extending our spatial product mixture models to the spatio-temporal context. This may be performed by either incorporating temporal dependence in the fully spatially dependent latent parameter, \mathbf{X}_{2t} , or by introducing space-time dependence in the other latent parameter vector, \mathbf{X}_{3t} . In the space-time context, products of more than three latent processes with distinct spatio-temporal characteristics may also be envisioned, and it would be interesting to explore how to further generalize our construction to capture different asymptotic regimes in space and time.

References

- Atchadé, Y. F. (2006) An adaptive version for the Metropolis adjusted Langevin algorithm with a truncated drift. Methodology and Computing in applied Probability **8**(2), 235–254.
- Bacro, J.-N., Gaetan, C., Opitz, T. and Toulemonde, G. (2020) Hierarchical space-time modeling of asymptotically independent exceedances with an application to precipitation data. Journal of the American Statistical Association **115**(530), 555–569.
- Banerjee, S., Carlin, B. P. and Gelfand, A. E. (2014) Hierarchical Modeling and Analysis for Spatial Data. Second edition. CRC Press.
- Breiman, L. (1965) On some limit theorems similar to the arc-sin law. Theory of Probability & Its Applications **10**(2), 323–331.
- Bücher, A. and Zhou, C. (2021) A horse race between the block maxima method and the peak–over–threshold approach. Statistical Science **36**(3), 360–378.
- Castro-Camilo, D., Huser, R. and Rue, H. (2019) A spliced Gamma-generalized Pareto model for short-term extreme wind speed probabilistic forecasting. Journal of Agricultural, Biological and Environmental Statistics **24**(3), 517–534.
- Clark, N. J. and Dixon, P. M. (2021) A class of spatially correlated self-exciting statistical models. Spatial Statistics **43**, 100493.
- Cooley, D., Cisewski, J., Erhardt, R. J., Jeon, S., Mannshardt, E., Omolo, B. O. and Sun, Y. (2012) A survey of spatial extremes: Measuring spatial dependence and modeling spatial effects. REVSTAT **10**(1), 135–165.
- Cooley, D., Nychka, D. and Naveau, P. (2007) Bayesian spatial modeling of extreme precipitation return levels. Journal of the American Statistical Association **102**(479), 824–840.
- Cressie, N. A. C. (1993) Statistics for Spatial Data. Wiley Online Library.
- Davison, A. C. and Huser, R. (2015) Statistics of Extremes. Annual Review of Statistics and its Application **2**, 203–235.
- Davison, A. C., Huser, R. and Thibaud, E. (2019) Spatial extremes. In Handbook of Environmental and Ecological Statistics, eds A. E. Gelfand, M. Fuentes, J. A. Hoeting and R. L. Smith, pp. 711–744. Boca Raton: CRC press.

- Davison, A. C., Padoan, S. and Ribatet, M. (2012) Statistical modelling of spatial extremes (with Discussion). Statistical Science **27**(2), 161–186.
- Davison, A. C. and Smith, R. L. (1990) Models for exceedances over high thresholds (with discussion). Journal of the Royal Statistical Society: Series B (Statistical Methodology) **52**(3), 393–442.
- Deng, W., Zhang, X., Liang, F. and Lin, G. (2018) Bayesian Deep Learning via stochastic gradient MCMC with a stochastic approximation adaptation. In Proceedings of the International Conference on Learning Representations 2019 Conference, pp. 1–18.
- de Fondeville, R. and Davison, A. C. (2018) High-dimensional peaks-over-threshold inference. Biometrika **105**(3), 575–592.
- Gneiting, T. and Raftery, A. E. (2007) Strictly proper scoring rules, prediction, and estimation. Journal of the American statistical Association **102**(477), 359–378.
- Hazra, A., Huser, R. and Jóhannesson, Á. V. (2021) Latent Gaussian models for high-dimensional spatial extremes. In Statistical Modeling Using Latent Gaussian Models – With Applications in Geophysics and Environmental Sciences, pp. 1–33. Expected to be published by Springer in 2022.
- Huser, R. and Wadsworth, J. L. (2019) Modeling spatial processes with unknown extremal dependence class. Journal of the American Statistical Association **114**, 434–444.
- Huser, R. and Wadsworth, J. L. (2020) Advances in statistical modeling of spatial extremes. Wiley Interdisciplinary Reviews: Computational Statistics p. e1537.
- Jóhannesson, Á. V., Siegert, S., Huser, R., Bakka, H. and Hrafnkelsson, B. (2021) Approximate Bayesian inference for analysis of spatio-temporal flood frequency data. Annals of Applied Statistics, To appear.
- Lerch, S., Thorarinsdottir, T. L., Ravazzolo, F. and Gneiting, T. (2017) Forecaster’s dilemma: extreme events and forecast evaluation. Statistical Science **32**(1), 106–127.
- Neal, R. M. (2011) MCMC using Hamiltonian dynamics. In Handbook of Markov Chain Monte Carlo, eds G. L. J. S. Brooks, A. Gelman and X.-L. Meng, chapter 5, pp. 113–162. Chapman & Hall/CRC.

- Neal, R. M. (2012) Bayesian Learning for Neural Networks. Volume 118. Springer Science & Business Media.
- Nemeth, C. and Fearnhead, P. (2020) Stochastic gradient Markov chain Monte Carlo. Journal of the American Statistical Association **116**(533), 433–450.
- Opitz, T., Huser, R., Bakka, H. and Rue, H. (2018) INLA goes extreme: Bayesian tail regression for the estimation of high spatio-temporal quantiles. Extremes **21**(3), 441–462.
- Resnick, S. I. (1987) Extreme Values, Regular Variation and Point Processes. Springer.
- Ribatet, M., Cooley, D. and Davison, A. C. (2012) Bayesian inference from composite likelihoods, with an application to spatial extremes. Statistica Sinica **22**, 813–845.
- Roberts, G. O. and Rosenthal, J. S. (1998) Optimal scaling of discrete approximations to Langevin diffusions. Journal of the Royal Statistical Society: Series B (Statistical Methodology) **60**(1), 255–268.
- Roberts, G. O. and Tweedie, R. L. (1996) Exponential convergence of Langevin distributions and their discrete approximations. Bernoulli **2**(4), 341–363.
- Sang, H. and Gelfand, A. E. (2009) Hierarchical modeling for extreme values observed over space and time. Environmental and Ecological Statistics **16**(3), 407–426.
- Sang, H. and Gelfand, A. E. (2010) Continuous spatial process models for spatial extreme values. Journal of Agricultural, Biological, and Environmental Statistics **15**(1), 49–65.
- Thibaud, E. and Opitz, T. (2015) Efficient inference and simulation for elliptical Pareto processes. Biometrika **102**(4), 855–870.
- Turkman, K. F., Turkman, M. A. and Pereira, J. (2010) Asymptotic models and inference for extremes of spatio-temporal data. Extremes **13**(4), 375–397.
- Welling, M. and Teh, Y. W. (2011) Bayesian learning via stochastic gradient Langevin dynamics. In Proceedings of the 28th International Conference on Machine Learning (ICML-11), pp. 681–688.
- Yadav, R., Huser, R. and Opitz, T. (2021) Spatial hierarchical modeling of threshold exceedances using rate mixtures. Environmetrics **32**(3), e2662.

Zhang, L., Shaby, B. A. and Wadsworth, J. L. (2021) Hierarchical transformed scale mixtures for flexible modeling of spatial extremes on datasets with many locations. Journal of the American Statistical Association, To appear.

Zhang, R., Li, C., Zhang, J., Chen, C. and Wilson, A. G. (2020) Cyclical stochastic gradient MCMC for Bayesian deep learning. In Proceedings of the International Conference on Learning Representations 2020 Conference, pp. 1–27.